

# Predicting Properties of Quantum Systems with Conditional Generative Models

Haoxiang Wang,<sup>1,2,\*</sup> Maurice Weber,<sup>3,4,\*</sup> Josh Izaac,<sup>4</sup> and Cedric Yen-Yu Lin<sup>2</sup>

<sup>1</sup>*University of Illinois Urbana-Champaign, Urbana, IL 61801, USA*

<sup>2</sup>*AWS Quantum Technologies, Seattle, WA 98170, USA*

<sup>3</sup>*ETH Zürich, Department of Computer Science, 8092 Zürich, Switzerland*

<sup>4</sup>*Xanadu, Toronto, ON, M5G 2C8, Canada*

Machine learning has emerged recently as a powerful tool for predicting properties of quantum many-body systems. For many ground states of gapped Hamiltonians, generative models can learn from measurements of a single quantum state to reconstruct the state accurately enough to predict local observables. Alternatively, kernel methods can predict local observables by learning from measurements on different but related states. In this work, we combine the benefits of both approaches and propose the use of conditional generative models to simultaneously represent a family of states, by learning shared structures of different quantum states from measurements. The trained model allows us to predict arbitrary local properties of ground states, even for states not present in the training data, and without necessitating further training for new observables. We numerically validate our approach (with simulations of up to 45 qubits) for two quantum many-body problems, 2D random Heisenberg models and Rydberg atom systems.

## I. INTRODUCTION

By harnessing the power of quantum mechanics, quantum computing has the potential to facilitate scientific discoveries and tackle various technological challenges. One of the most promising applications of quantum computing is to solve quantum many-body problems, a cornerstone task in multiple scientific disciplines, including physics, chemistry, and materials science [5]. While classical methods such as density functional theory [16], density-matrix renormalization group (DMRG) [59], and quantum Monte Carlo [20] have brought significant advancements in the study of certain systems of interest, they typically do not scale to large system sizes for general quantum mechanical systems. In contrast, due to their intrinsically quantum mechanical nature, quantum computers are expected to be able to simulate large-scale quantum many-body systems in the near future [5, 6]. The utility of such approaches crucially hinges on the ability to extract useful information from the simulated system by means of measuring multiple identical copies and subsequent statistical post-processing of the obtained measurements. The task of complete characterization of the quantum state of interest is known as quantum state tomography (QST) [22, 28, 47, 57]. However, for generic systems, exact tomographic techniques scale unfavorably with system size and become impractical as the number of qubits increases [30, 41]. In cases where one is interested only in a limited number of observables of the state, shadow tomography [1, 3, 11, 31–33] is a promising alternative to full-state tomography, alleviating the requirement to prepare an exponential number of copies of the state. Shadow tomography nevertheless has its limitations (on modern NISQ machines), e.g., in the case of global observables [32].

Machine learning (ML) has emerged as a powerful and general technique for QST in regimes where a limited amount of experimental data is available [2, 19, 46, 53]. In this context, restricted Boltzmann machines (RBM) have been studied extensively and were shown to be able to learn accurate representations of states whose evolution can be simulated in polynomial time using classical methods [53]. The representational power of deep Boltzmann machines (DBM) with complex weights has been studied theoretically in Ref. [27], where it has been proven that these approaches can efficiently represent most quantum states. While theoretically encouraging, DBMs with complex weights remain of limited practical value, due to the intrinsic difficulties of efficiently sampling from such models. In response, other deep architectures have been explored, including recurrent neural networks (RNN) [18], variational autoencoders [46] and transformer networks [21]. These results point to the encouraging observation that these proposed neural networks have sufficient representational power to learn some complex quantum states. However, when the task is to learn representations of a *family of quantum states*, these neural networks have to be re-trained on each state of the family to encode the state.

In an orthogonal line of research, ML has been used to directly predict phases of matter of quantum systems [18, 43, 55]. These ML models are trained on measurement outcomes from many related quantum systems, and then used to predict phases of matter for unseen quantum systems from the same family; in contrast to QST, these techniques do not aim to learn a representation of the quantum states of interest. Huang et al. [34] take this a step further to estimate arbitrary local (i.e., few-body) observables, by combining a kernel-based learning approach with classical shadows. Specifically, given a collection of classical shadows obtained from performing random Pauli measurements on many different but related quantum states, this technique allows predicting the expectation of any local observable. In addition,

---

\* Equal contribution (alphabetic order).

Huang et al. [34] provide rigorous guarantees for the classical representation obtained via kernel methods. As for numerical experiments, the authors of [34] fit an individual model for each observable, separately. Notably, while kernel methods enable rigorous guarantees, they usually empirically underperform neural networks in modern ML tasks [7, 51].

Here, we build on these previous works, and propose a framework for learning classical representations of a family of quantum states using machine learning (ML) models. To that end, we propose an ML-based method to post-process measurement statistics of multiple quantum states *jointly* and exploit the shared structure between these states, such as, e.g., ground states of a family of quantum many-body Hamiltonians. This reduces the experimental and computational burden from at least two angles. Firstly, similar to Ref. [34], our technique enables experimentalists and practitioners to reduce measurement costs and even study properties of states for which no measurements are available, including states that cannot be prepared on modern NISQ hardware. However, in contrast to Ref. [34], our technique learns a representation of the family of states and allows us to generate new samples. Secondly, similar to ML-based QST [19, 46, 53], we encode the full state in a generative model that allows us to predict arbitrary properties of the states by sampling from the model, alleviating the need to train a model for each property from scratch. In contrast to ML-based QST, our model is not restricted to a single state, but also generalizes to related states for which no measurements have been obtained.

In numerical simulations (of up to 45 qubits) of the 2D anti-ferromagnetic random Heisenberg model (Sec. III A) and Rydberg atom systems (Sec. III B), we show that our conditional generative models are able to accurately represent new ground states and predict their properties such as subsystem entanglement entropy, correlation functions, and quantum phases. Notably, with proof-of-concept numerical examples (Sec. III B 2, III B 3), we demonstrate that our model can potentially allow experimentalists and practitioners to predict properties of systems beyond current hardware limits (e.g., large-scale quantum systems that modern quantum computers cannot simulate).

## II. REPRESENTING QUANTUM STATES WITH CONDITIONAL GENERATIVE MODELS

In this work, we consider  $n$ -qubit quantum states  $\rho(\mathbf{x})$  to be density operators acting on a  $d$ -dimensional complex Hilbert space  $\mathcal{H}$ , with  $d = 2^n$ . The density operators are parametrized by a real-valued parameter  $\mathbf{x} \in \mathbb{R}^m$ . The most general type of measurement allowed by quantum mechanics is positive operator-valued measures (POVM). A POVM is a collection of positive semidefinite linear operators  $\mathcal{M} = \{M_{\vec{a}}\}_{\vec{a}}$  which resolve the identity  $\sum_{\vec{a}} M_{\vec{a}} = 1$ . Each POVM operator  $M_{\vec{a}}$  cor-

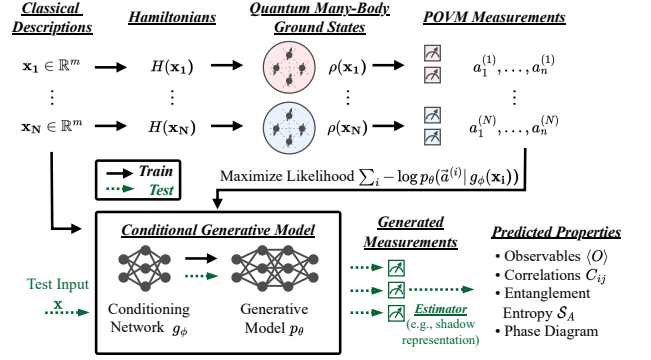


FIG. 1. Overview of our framework. The training pipeline of the conditional generative model is marked with solid black arrows, while the test pipeline is marked with dashed green arrows.

responds to a measurement outcome  $\vec{a} = (a_1, \dots, a_n)$  whose probability is obtained from Born's rule,

$$p(\vec{a} | \mathbf{x}) = \text{Tr}[M_{\vec{a}} \rho(\mathbf{x})]. \quad (1)$$

To fully represent a generic quantum state  $\rho$ , we need to use an informationally complete (IC) POVM; that is, the POVM must consist of at least  $d^2$  elements which span the space of self-adjoint operators on  $\mathcal{H}$ . This implies that the measurements collected from an IC POVM contain the necessary statistical information to fully characterize the state. In this work, in the context of the Heisenberg model, we focus on the Pauli-6 POVM consisting of  $n$ -qubit tensor products of projections to the eigenspaces of the Pauli observables [19]<sup>1</sup>. This POVM corresponds to performing measurements in one of the three Pauli bases, uniformly at random. For the Rydberg atom systems, we make measurements in the computational basis (i.e.,  $Z$ -basis) as this POVM is sufficient for characterizing ground states of the Rydberg systems considered here. We remark that our proposed framework is not restricted to these choices of POVMs (other POVMs can also be adopted). Among different ways to estimate properties like expectation values or entanglement entropies, we adopt the classical shadow protocol [32] due to its simplicity and statistical guarantees.

For a family of states  $\rho(\mathbf{x})$  indexed by the parameter  $\mathbf{x}$ , our dataset consists of a collection of measurement statistics and parameters,  $\mathcal{D} = \{(\vec{a}^{(1)}, \mathbf{x}^{(1)}), \dots, (\vec{a}^{(N)}, \mathbf{x}^{(N)})\}$ , and we train a generative model  $p_{\theta}$ , parameterized as a neural network, to maximize the likelihood of the observed measurements. To condition the model distribution  $p_{\theta}$  on the classical parameter  $\mathbf{x}$ , we use an embedding  $\mathbf{x} \mapsto g_{\phi}(\mathbf{x})$  with trainable parameters  $\phi$  and use this as an additional input to

<sup>1</sup> We refer the reader to Appendix C 1 for details about the Pauli-6 POVM.

the model  $p_\theta$ . To make the optimization and sampling process tractable, we decompose the joint distribution into a product of conditional distributions in an autoregressive manner,

$$p_{\theta,\phi}(a_1, \dots, a_n | \mathbf{x}) = \prod_{i=1}^n p_\theta(a_i | a_{i-1}, \dots, a_1, g_\phi(\mathbf{x})), \quad (2)$$

where  $\theta$  denotes the set of parameters of the generative model, and  $\phi$  are the parameters of the embedding network. Since both the embedding  $g_\phi$  and the generative model  $p_\theta$  are parametrized as neural networks, they can be trained in an end-to-end manner.

**Training.** To train the model, we sample  $N_H$  Hamiltonians (each of a unique parameter  $\mathbf{x} \in \mathbb{R}^m$ ) and obtain  $N_s$  measurement outcomes for each ground state  $\rho(\mathbf{x})$ . Each measurement outcome is a training sample, leading to a training set  $\mathcal{D}$  of size  $N_H N_s$ . As our training objective, we minimize the average negative log-likelihood loss over training data,

$$\min_{\theta,\phi} \mathcal{L}(\theta, \phi) := \frac{1}{N_H N_s} \sum_{(\tilde{\mathbf{a}}, \mathbf{x}) \in \mathcal{D}} -\log p_{\theta,\phi}(a_1, \dots, a_n | \mathbf{x}), \quad (3)$$

what corresponds to maximizing the (conditional) likelihoods over the observed measurement outcomes.

**Prediction.** Once the model is trained, measurements for a new state of the same family (e.g., ground state of a related Hamiltonian) can be generated by conditioning it on the classical variable. Based on these generated measurements, arbitrary properties of the unknown state can be predicted using estimation protocols such as shadow tomography [32]. A schematic diagram of our framework is presented in Figure 1.

### III. LEARNING GROUND STATES OF QUANTUM MANY-BODY HAMILTONIANS

In this section, we present our results for two quantum many-body problems, 2D random Heisenberg models and Rydberg atom systems, where each problem includes a family of Hamiltonians. Our model can learn from ground-state measurements of multiple Hamiltonians, and be used to predict ground-state properties of other Hamiltonians from the same family. For 2D random Heisenberg models, our proposed conditional generative model (CGM) consists of i) a graph convolutional network (GCN) [37] which takes the classical description of the Hamiltonian as input, and ii) a transformer [56] as the generative model to represent quantum states and generate measurements. For Rydberg atom systems, we use a linear projection instead of a GCN to condition on system parameters, and continue to use a transformer as the generative model. In both cases, our implementations

are publicly available<sup>2</sup>.

#### A. 2D anti-ferromagnetic random Heisenberg model

The first family of Hamiltonians we consider is the 2D anti-ferromagnetic random Heisenberg model, where qubits, i.e., spin-1/2 particles, are allocated over a square lattice. Specifically, we are interested in the ground state of the Hamiltonians

$$H(\mathbf{x}) = \sum_{\langle ij \rangle} \mathbf{x}_{ij} (X_i X_j + Y_i Y_j + Z_i Z_j), \quad (4)$$

where  $\langle ij \rangle$  represents nearest-neighbor interactions and the summation is over all possible pairs on this lattice. For each pair  $\langle ij \rangle$ , the corresponding interaction strength  $\mathbf{x}_{ij}$  is uniformly sampled from the interval  $[0, 2]$ . The Hamiltonian in Eq. (4) can be described by a weighted undirected graph without any loss of information. Each qubit is expressed as a node, and the coupling strength between two sites corresponds to a weighted edge in the graph. Denoting the adjacency matrix of the graph as  $\mathbf{x}$ , we write  $\rho(\mathbf{x})$  for the ground states of the Hamiltonian corresponding to the grid lattice defined by the graph  $\mathbf{x}$ .

**Model Structure.** To exploit the full classical information contained in the graph structure of the Hamiltonian, we use a graph convolutional network (GCN) [37], followed by a linear projection layer to get a trainable embedding of the graph,  $\mathbf{x} \mapsto g_\phi(\mathbf{x})$ . As for the generative model, we adopt the transformer architecture [56], which has shown tremendous success for sequence modeling in the context of natural language processing [15, 23], computer vision [39] and also for quantum state tomography [21]. We condition the transformer on the Hamiltonian by adding the graph embedding vector  $g_\phi(\mathbf{x})$  to the encoded measurements after the positional encoding. The model structure is illustrated in Figure 2, and more details are provided in Appendix A 1.

**Estimation Protocol.** Given a trained model for a fixed lattice size, we evaluate it by sampling from the model distribution (2) and estimate properties using the classical shadow protocol [32]. Specifically, given a collection of  $N$  artificial measurements outcomes generated by the model,  $\vec{b}^{(1)}, \dots, \vec{b}^{(N)}$ , the resulting shadow state can be expressed as

$$\hat{\rho}(\mathbf{x})_{\text{model}} = \frac{1}{N} \sum_{i=1}^N \bigotimes_{j=1}^n \left( 3|b_j^{(i)}\rangle\langle b_j^{(i)}| - \mathbb{1}_2 \right) \quad (5)$$

where the kets  $|b_j^{(i)}\rangle$  correspond to the eigenstate associated with the measurement outcome  $b_j^{(i)}$  sampled by the

<sup>2</sup> <https://github.com/PennyLaneAI/generative-quantum-states>





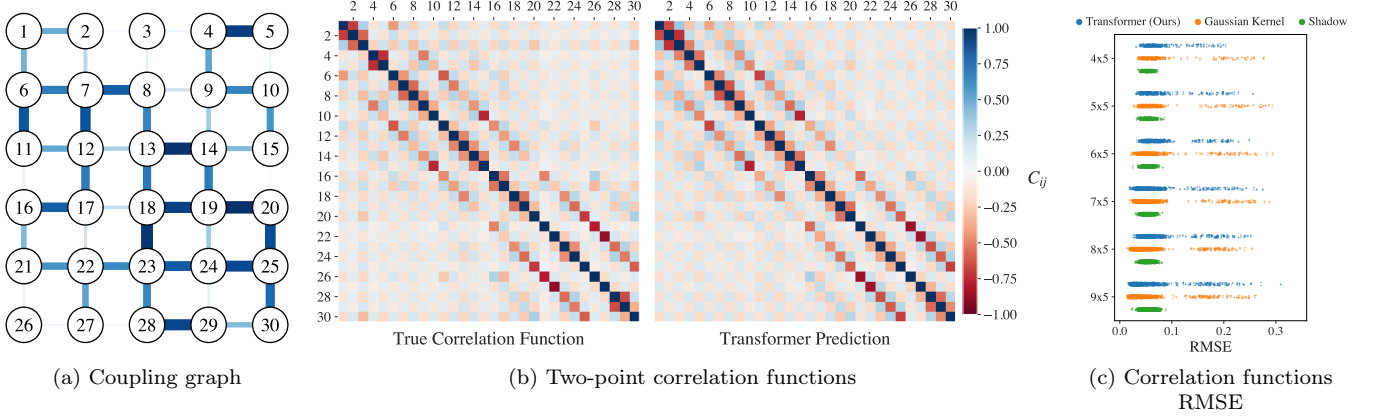


FIG. 3. Predicting correlation functions of ground states of the 2D random anti-ferromagnetic Heisenberg model. a) Random Coupling graph from the test set. The graph determines the 2D random Heisenberg model (4), and is used to condition our generative model. The interaction strength is indicated by both thickness and color (thicker and darker means higher interaction strength). b) True and predicted two-point correlation functions (6) for a ground state from the test set encoded by our generative model given the coupling graph. c) Root Mean Square Error (RMSE) between true and predicted correlation functions for systems of different sizes, for our conditional generative model (blue), Gaussian kernel (orange), and shadow tomography (green). Each point in the plot corresponds to the error of correlation predictions for different sites, averaged over Hamiltonians from the test set.

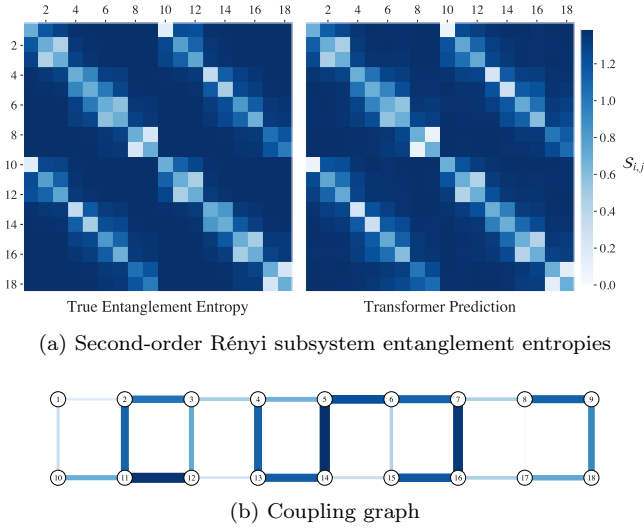


FIG. 4. a) Second-order Rényi subsystem entanglement entropies for subsystems of size at most two (7). The conditional generative model is conditioned on the coupling graph in (b), which determines the Hamiltonian (4) of the 2D random Heisenberg model. The strength of the couplings is indicated by the width and color of the edges in the graph.

two. This property is defined by

$$\mathcal{S}(\rho_A) = -\log \text{Tr}[\rho_A^2], \quad (7)$$

where  $\rho_A$  is the reduced density matrix of the subsystem  $A$ . Since this quantity can be rewritten in terms of the expectation value of the local swap operator, the statistical guarantees of the classical shadow protocol imply that the required number of samples scales exponentially

only in the subsystem size [32], allowing one to compute  $\mathcal{S}(\rho_A)$  efficiently using classical shadows for small subsystems. Fig. 4 shows the true and predicted entanglement entropies for the Hamiltonian defined by the (randomly sampled) coupling graph shown in Fig. 4b. The predictions are obtained analogously to the correlation functions (i.e., sampling from the conditional generative transformer, constructing the classical shadow, and predicting the property based on the shadow). Similar to the correlation functions, we see from the figure that the model makes fairly accurate predictions in comparison with the true entanglement entropies. Fig. 5 shows the distribution of RMSE for the entanglement entropies. Each point corresponds to a particular subsystem and shows the averaged RMSE over Hamiltonians from the test set (left panel) and the train set (right panel), respectively. Similar to the correlation functions, our approach leads to RMSEs with a higher variance compared to classical shadows, although here the distribution is skewed more towards zero, implying that our predictions are more accurate than the classical shadow predictions. Finally, in comparison with the Gaussian kernel, we can see that our generative model approach performs significantly better, throughout all system sizes. Interestingly, these observations hold both for the training and the testing errors.

## B. Rydberg atom systems

The second family of Hamiltonians we consider is Rydberg atom systems. Trapped Rydberg atoms are a class of highly controllable neutral atoms that can be

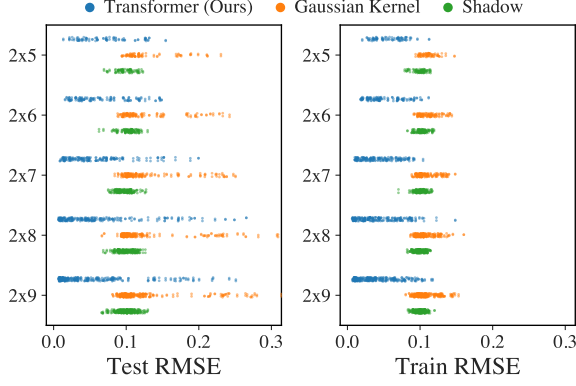


FIG. 5. RMSE between true and predicted entanglement entropy for subsystems of size at most two, for our conditional generative model (blue), Gaussian kernel (orange), and shadow tomography (green). For a given system size, each point in the plot corresponds to the error of the entropy prediction for a particular subsystem, averaged over Hamiltonians from the test set.

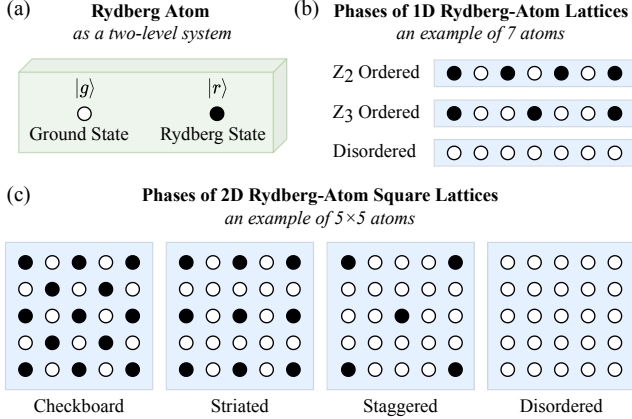


FIG. 6. Rydberg atom systems. (a) A Rydberg atom can be viewed as a two-level system, with the ground state  $|g\rangle$  and Rydberg state  $|r\rangle$  (an excited state). (b) Three quantum phases of 1D lattices of equidistant Rydberg atoms, in an example of 7 atoms. (c) Four quantum phases of 2D square lattices of Rydberg atoms, in an example of  $5 \times 5$  atoms (the staggered phase shown here is a little different from that of Ref. [48] due to the boundary effect of this relatively small  $5 \times 5$  lattice).

used to build programmable Ising-type quantum simulators [10, 25, 49, 50]. In such simulations, a Rydberg atom is effectively a two-level system consisting of a ground state  $|g\rangle$  and an excited state  $|r\rangle$ , where  $|r\rangle$  is typically the  $70S_{1/2}$  Rydberg state of neutral  $^{87}\text{Rb}$  atoms. Rydberg atoms can be allocated on a plane and trapped by light tweezers. In [10], Rydberg atoms are placed along a 1D lattice (i.e., a chain) equidistantly, while [25] allocates the atoms on a 2D square lattice. For either a 1D or a 2D lattice of Rydberg atoms, the Hamiltonian of such a

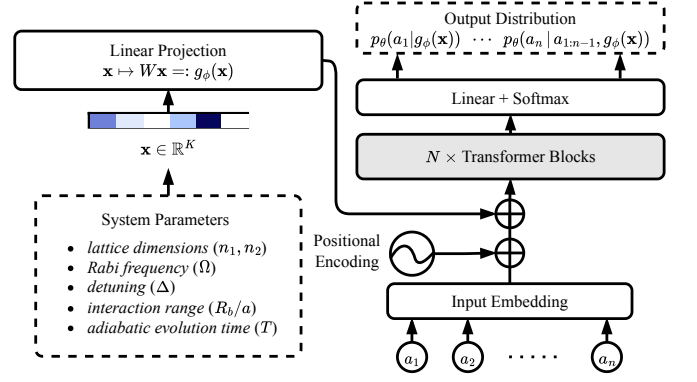


FIG. 7. Structure of the conditional generative model for Rydberg atom systems.

system can be written as

$$H = \frac{\Omega}{2} \sum_i X_i - \Delta \sum_i N_i + \sum_{i < j} \frac{V_0}{|\vec{x}_i - \vec{x}_j|^6} N_i N_j, \quad (8)$$

where  $\Omega$  is the Rabi frequency,  $\Delta$  is the detuning of a laser,  $V_0$  is the Rydberg interaction constant, and  $\vec{x}_i$  is the position vector of the site  $i$ .  $N_i = |r_i\rangle\langle r_i| = (1 + Z_i)/2$  is the occupation number operator at site  $i$ , where  $Z_i$  and  $X_i = |r_i\rangle\langle g_i| + |g_i\rangle\langle r_i|$  are pseudo-Pauli operators. Following prior works [10, 25, 34], we consider all atoms to be equidistantly distributed over a 1D chain or a 2D square lattice, and refer to the nearest-neighbor distance as the atom separation  $a$ . We define  $R_0 = (V_0/\Omega)^{1/6}$ , and then use  $R_0/a$  as a parameter for the Rydberg-atom phase diagram (e.g., Fig. 8, 9) following the convention of prior studies [10, 25, 34].

**Ground State Preparation.** Following recent experimental work on programmable Rydberg quantum simulators [10, 25, 49, 50], we approximately prepare the ground state using adiabatic evolution [4]. Initially, each Rydberg atom is prepared in its own ground state  $|g\rangle$ , which globally corresponds to the ground state  $|g \dots g\rangle$  of the Hamiltonian Eq. (8) with a large negative detuning  $\Delta$  and zero-valued  $\Omega$ . We then evolve the state under the time-dependent Hamiltonian Eq. (8) while linearly increasing the detuning strength  $\Delta$ , and subsequently the Rabi frequency  $\Omega$ , to desired positive values. The adiabatic theorem [14] implies that with a slow enough evolution, the final state should remain in the ground state of the final Hamiltonian.

**Estimation Protocol.** Current experimental realizations of Rydberg quantum computers only support measurements in the computational basis (i.e.,  $Z$ -basis), and therefore a hardware implementation would not be able to utilize the full classical shadow approach for state tomography. We instead follow the approach suggested by [54]: without loss of generality, we may assume  $\Omega > 0$  by a suitable global phase rotation, which (by the Perron-Frobenius theorem) implies the ground state can be chosen to have positive real coefficients. We will therefore

make the approximation that the ground state preparation procedure produces a state with real amplitudes; this should be a good approximation if the adiabatically-prepared state is close to the ground state. This allows the states we study to be uniquely characterized by measurements in the computational basis.

**Dataset.** To generate a dataset for training and evaluation, we use the `Bloqade.jl` [45] package to prepare ground states of Rydberg Hamiltonians with adiabatic evolution (i.e., tuning  $\Omega$  and  $\Delta$  gradually across time), following practices of prior experimental works [10, 25]. Since ground states of Rydberg systems can be fully determined in the computational basis, for each numerically prepared state, we generate 1000 measurements in the computational basis. Overall, we conduct simulations for 1D and 2D Rydberg atom lattices, varying the lattice dimensions, atom separation  $a$  (i.e., the distance between nearest neighbors), and the total adiabatic evolution time  $T$ . More details about the numerical simulations (e.g., schedulers of  $\Omega$  and  $\Delta$ ) are provided in Appendix C 2.

**Model Structure.** In contrast to the 2D random Heisenberg models in Sec. III A, a Rydberg atom system can be described by scalar parameters such as  $\Omega$ ,  $\Delta$  and the lattice dimensions, which can be concatenated into a vector  $\mathbf{x}$ . For this reason, we directly use a linear model that takes the vector  $x$  as input and maps it to an embedding  $g_\phi(\mathbf{x})$ . Similar to the Heisenberg model, we then condition a transformer on  $\mathbf{x}$  by adding  $g_\phi(\mathbf{x})$  to the embedding right after the positional encoding. We illustrate this model structure in Fig. 7.

### 1. Predicting quantum phases

The authors of Ref. [10] experimentally show that for 1D chains of Rydberg atoms, the ground states can exhibit several different quantum phases, including the disordered phase,  $Z_2$  ordered phase, and  $Z_3$  ordered phase. On the other hand, it has been shown in Ref. [25, 48] that the ground states of 2D square lattices of Rydberg atoms also have several quantum phases, such as disordered, checkboard, striated, and staggered phases. We provide illustrations for these phases in Fig. 6. For each prepared state, we apply order parameters of phases ( $O_{Z_2}, O_{Z_3}$  for 1D and  $O_{\text{checkboard}}, O_{\text{striated}}, O_{\text{staggered}}$  for 2D) repeatedly, and determine the phase of this state from estimated values of the order parameters. Detailed definitions of these order parameters are provided in Appendix B 2 b.

To evaluate our model, we set up a 31-atom 1D lattice and a 5x5-atom 2D square lattice, and simulate adiabatic evolutions for various choices of the atom separation  $a$ , yielding a collection of measurements in the computational basis. Based on these measurements, we construct the ground truth phase for both lattices, shown in Fig. 8a and Fig. 9a, respectively. To train our conditional generative model, we sample 100 parameter configurations over the phase diagram, where each configuration corre-

Dataset	Method	Prediction Errors	
		Phase (%)	Order Param.
Rydberg-1D (31 atoms)	Dirichlet Kernel [34]	15.21	0.1138
	Gaussian Kernel [34]	4.94	0.0547
	NTK [34]	4.18	0.0534
	Ours	<b>1.71</b>	<b>0.0199</b>
Rydberg-2D (5x5 atoms)	Dirichlet Kernel [34]	24.23	0.1192
	Gaussian Kernel [34]	10.99	0.1192
	NTK [34]	9.86	0.0965
	Ours	<b>4.51</b>	<b>0.0709</b>

TABLE I. Prediction results on 1D (31 atoms) and 2D (5x5 atoms) Rydberg atom lattices, with average prediction errors of **i)** phases (as a classification task so that the error is the classification error), and **ii)** order parameters of these phases (the error is computed in RMSE), with detailed definitions provided in Appendix B 2 b. **Bold** numbers indicate the lowest errors (lower is better) across these methods.

sponds to a ground state that we prepared numerically via adiabatic evolution. The measurements stemming from these states constitute our training set, which includes a total of 100k measurements. After training, we condition the model on the remaining parameter configurations to generate measurements from our model, corresponding to their ground states, in order to reconstruct the entire phase diagram. The phase diagrams predicted by our method are shown in Fig. 8b and Fig. 9b. It can be seen from the figure that they are very similar to the true phase diagrams. This indicates that our model is capable of encoding the ground states of the entire family of Rydberg Hamiltonians fairly accurately and generalizes to new systems (i.e., parameter configurations).

In addition, we compare our method against the three kernel methods of Ref. [34] for the phase prediction task over these 1D and 2D lattices. We compute the prediction errors of **i)** the classification of phases and **ii)** the order parameters of these phases (see Appendix B 2 b for details). The empirical results are provided in Table I. Clearly, our model significantly outperforms the three kernel methods used in Ref. [34], corroborating the power and effectiveness of our proposed method. One can observe that the Gaussian kernel and the neural tangent kernel (NTK) [35] perform much better than the Dirichlet kernel in both 1D and 2D cases. Hence, we present the phase diagrams predicted by Gaussian kernel and NTK in Fig. 8 and 9 for comparison.

### 2. Predicting phases of larger quantum systems

Modern quantum devices can only simulate intermediate-scale quantum systems, while physicists are interested in systems of larger scales in many cases. Here we use 1D Rydberg lattices as a showcase to demonstrate that our method can be used to predict

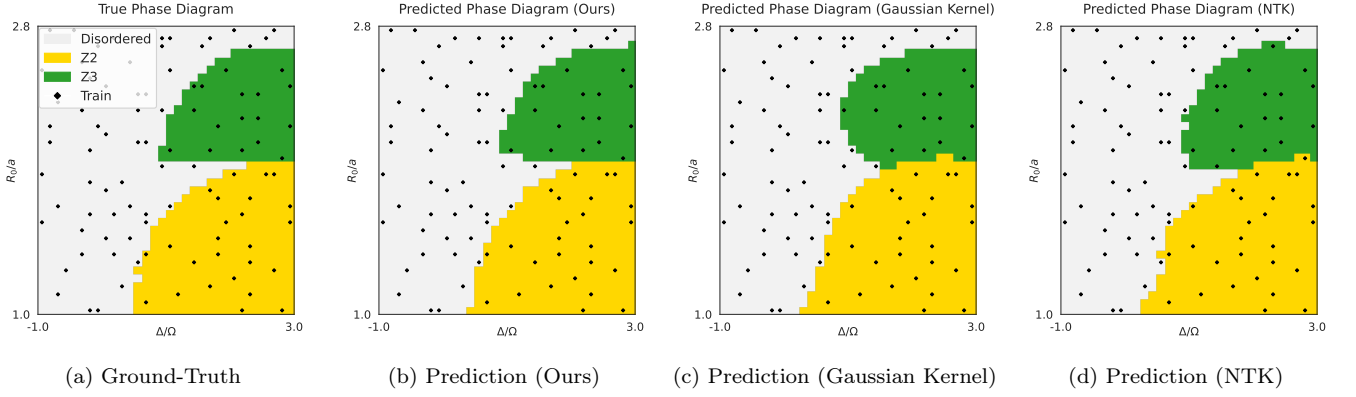


FIG. 8. Predicting phases of ground states of **1D** Rydberg atom lattices (31 atoms). a) Ground-truth phase diagram. b) Predicted phase diagram by our conditional generative model. c) Predicted phase diagram by Gaussian kernel. d) Predicted phase diagram by Neural Tangent Kernel (NTK).

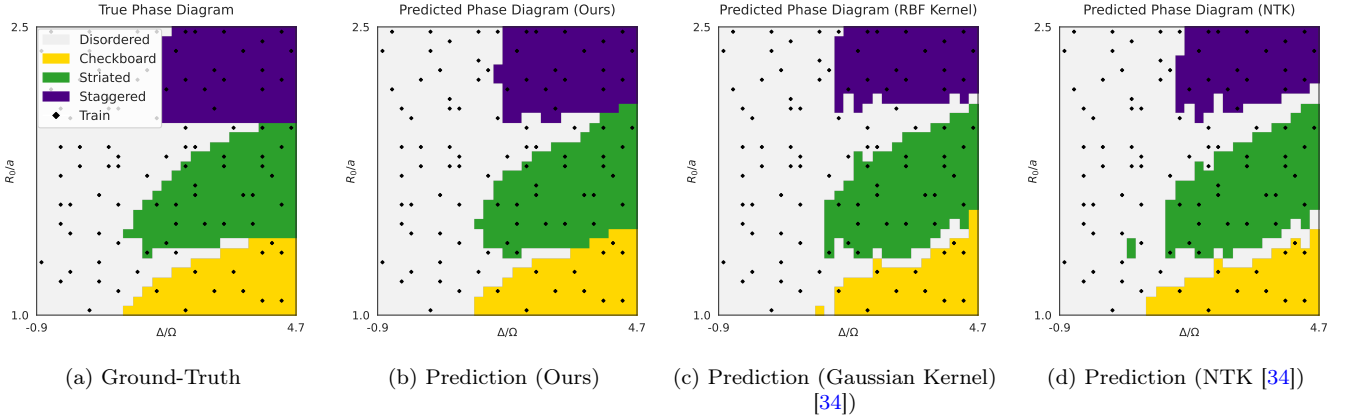


FIG. 9. Predicting phases of ground states of **2D** Rydberg atom lattices (5x5 atoms) a) Ground-truth phase diagram. b) Predicted phase diagram by our conditional generative model. c) Predicted phase diagram by Gaussian kernel. d) Predicted phase diagram by Neural Tangent Kernel (NTK).

properties of larger quantum systems (i.e., larger than any system in the training set). Specifically, we consider the phase prediction task for ground states of 1D Rydberg lattices. We collect ground-state measurements from 1D Rydberg lattices of  $13, 15, 17, \dots, 2k+1, \dots, 29$  atoms, and train our model over these data. Then, we ask the model to predict the phase diagram of 1D Rydberg lattices of 31 and 33 atoms, which are larger than those in the training set. The true phase diagrams of these lattices are plotted in Fig. 10a. A special phenomenon one can easily observe from Fig. 10a is the periodic emergence of the  $Z_3$  phase; the  $Z_2$  phase stably appears in the phase diagrams for lattices of  $2k+1$  atoms, and the  $Z_3$  phase only stably appears as the lattice has  $3k+1$  atoms, where  $k$  is any positive integer. Hence, to predict phases accurately for larger systems, a machine learning model must discover and understand this phenomenon.

From Fig. 10b, we can see that our model predicts (i) the emergence of the  $Z_3$  phase for 31 atoms and (ii) the disappearance of the  $Z_3$  phase for 33 atoms. Notice that our model only saw  $Z_3$  phases only for 19 and 25

atoms during training. This result implies that our proposed model is indeed able to predict certain properties for systems whose sizes exceed the training systems. In comparison, Fig. 10c and 10d show that the kernel methods used in Ref. [34] cannot predict the emergence of the  $Z_3$  phase for 31 atoms, after being trained on the same dataset as our model.

### 3. Predicting phases of ground states prepared with longer adiabatic evolution time

The ground-state preparation of Rydberg atoms via adiabatic evolution needs a sufficiently long evolution time to reach the exact many-body ground state. Otherwise, the prepared state becomes an excited state (possibly of low energy) instead. Typically, the longer the evolution is, the more accurate the preparation becomes. However, currently, Rydberg-atom experiments can only endure for a few microseconds [13, 24], leading to inaccurate adiabatically prepared states in many cases. Thus, predicting the properties of states prepared with longer



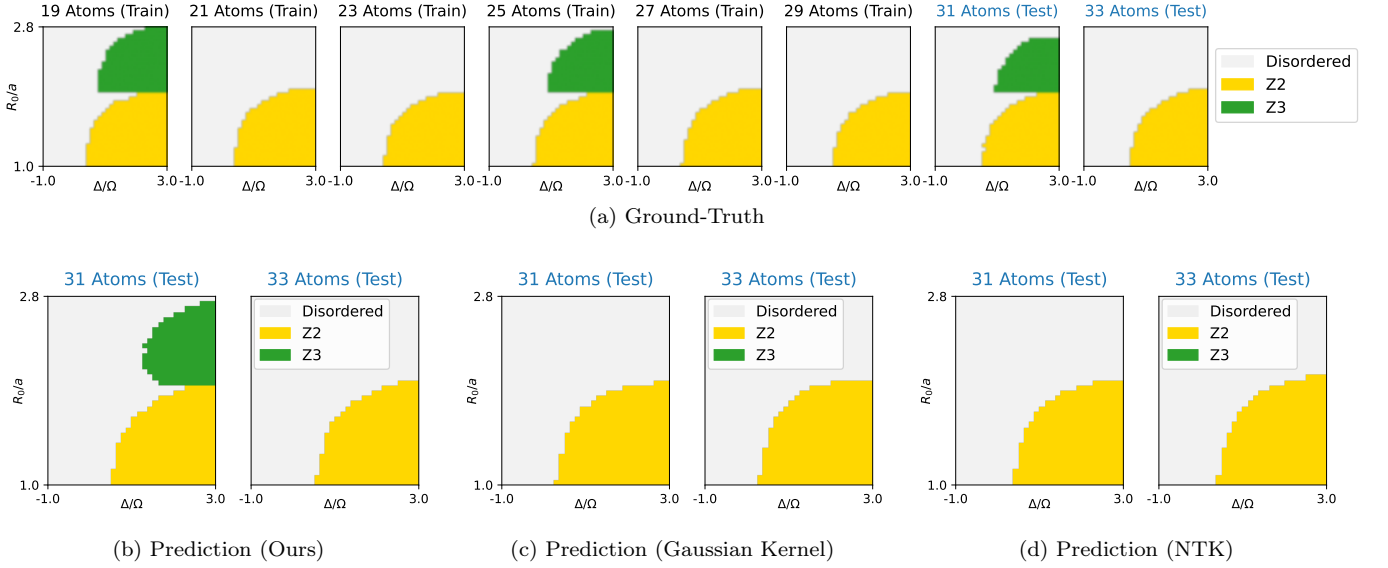


FIG. 10. Phase predictions for 1D Rydberg atom lattices of larger system sizes. (a) Ground-truth phase diagrams of 1D Rydberg atom lattices of increasing sizes, where the training set contains lattices of 13, 15, ..., 29 atoms & the test set includes lattices of 31 and 33 atoms. (b) The predicted phase diagrams of our method. Note that our method accurately predicts the emergence and disappearance of the  $Z_3$  phase in the 31-atom and 33-atom lattices, respectively. (c)(d) The predicted phase diagrams of two kernel methods used in [34], which fail at predicting the emergence of the  $Z_3$  phase for the 31-atom lattice.

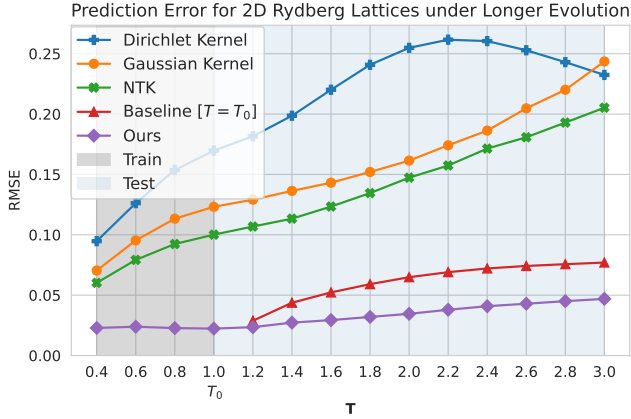


FIG. 11. Average prediction errors of phase order parameters for a 2D Rydberg lattice (5x5 atoms) simulated with longer adiabatic evolution times than  $T_0 = 1.0\mu s$ . Three order parameters,  $O_{\text{checkboard}}$ ,  $O_{\text{striated}}$ ,  $O_{\text{staggered}}$  (see Appendix B 2 b for definitions), are predicted, and the prediction errors are computed in RSME. Our method is compared with a baseline method, **Baseline** [ $T = T_0$ ] (using the ground-truth at  $T = T_0$  as the prediction for larger  $T$ ), and three kernel methods used in Ref. [34], Dirichlet, Gaussian, and neural tangent kernel (NTK), are compared in this experiment.

adiabatic evolution times can give practitioners a more accurate understanding of the target ground state.

Here, we consider a 2D Rydberg square lattice of 5x5 atoms, and study the predictive performance of our model for states prepared with longer evolution times.

The training set contains measurements for systems simulated with the total adiabatic evolution time,  $T \leq T_0 := 1.0\mu s$ . The trained conditional generative model is then used to predict phases of systems simulated with evolution times  $T > T_0 = 1.0\mu s$ . In Fig. 11, we plot the average prediction error of the trained model for the phase order parameters, and compare it with the baseline that keeps using the ground-truth phase diagram at  $T = T_0$ <sup>4</sup>. We can see from Fig. 11 that our trained model is able to predict the phases of Rydberg atom systems simulated with longer adiabatic evolution times more accurately than this baseline method (named as **Baseline** [ $T = T_0$ ] in Fig. 11), which directly uses the ground-truth phase diagram at  $T = T_0$  as prediction for any  $T > T_0$ . Also, our method outperforms kernel methods used in Ref. [34] significantly. The predicted phase diagrams by our method and the kernel methods for  $T = 3.0\mu s$  are provided in Fig. 12, and one can easily observe that our method's prediction is much more accurate compared with the kernel methods used by Ref. [34].

#### IV. DISCUSSION

The results presented in this work provide tangible evidence that state-of-the-art classical machine learning models have the capacity to learn accurate representations of entire families of quantum states. Using trainable embeddings to condition generative models on clas-

<sup>4</sup> This is the practice in real Rydberg atom experiments [25].

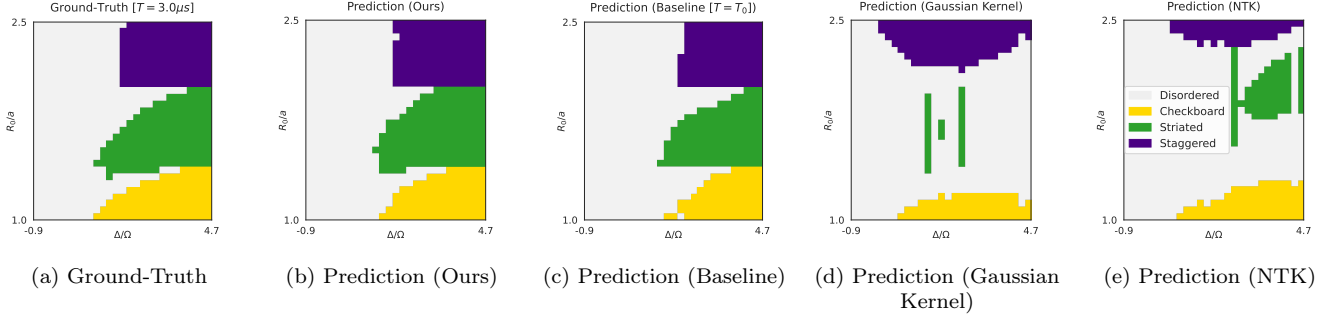


FIG. 12. Phase predictions for the 2D Rydberg atom lattice (5x5 atoms) as an adiabatic evolution of  $T = 3.0\mu s$ , while the models are being trained over lattices with adiabatic evolution time  $T \leq T_0 = 1.0\mu s$ . a) Ground-truth phase diagram as  $T = 3.0\mu s$ . b) Predicted phase diagram by our conditional generative model. c) Predicted phase diagram by the **Baseline** [ $T = T_0$ ] method, which uses the ground-truth at  $T = T_0$  as the prediction for larger  $T$ . d) Predicted phase diagram by Gaussian kernel. e) Predicted phase diagram by Neural Tangent Kernel (NTK).

sical parameters of the quantum system of interest, we have shown that the resulting generative models can be used to generate artificial measurement samples corresponding to states which were not present in the training set, and thereby predict properties like local observables, entanglement entropies, and phase diagrams. We have demonstrated our method on ground states of the two-dimensional anti-ferromagnetic Heisenberg model and Rydberg atom systems and shown remarkable improvements over related techniques based on shadow tomography and kernel methods. Throughout our numerical simulations, we have used the transformer architecture as our generative model, since it has shown promising success in sequence modeling. However, the complexity of transformers scales quadratically with the length of the input sequence, which potentially becomes problematic when the goal is to model long sequences with thousands of qubits. This poses exciting future research avenues where one could potentially explore other models like long-range transformers [44] or other ML models which are designed to model long-range dependencies such as state-space models [29, 38]. Furthermore, in this work, we have only explored our proposed method on numerically simulated quantum systems of intermediate scales (up to 45 qubits). It would be interesting to inves-

tigate the proposed method on larger quantum systems (e.g., Rydberg-atom quantum simulators of more than 200 atoms [25]), which would also expose our methods to various sources of imperfections like quantum noise and errors.

*Note.* During the completion of this work, a related approach has been released on arXiv [60], which, similar to our technique, uses transformers to represent a family of quantum states. Different from ours, they treat the conditioning variable as a separate element of the sequence and only consider vector-valued classical variables. Furthermore, they directly parametrize the wave function and minimize the variational energy of a Hamiltonian of interest. In this way, only pure states can be modeled, posing additional challenges when considering realistic quantum systems where noise and errors are prevalent.

## ACKNOWLEDGMENTS

The authors thank Mao Lin, Peter Komar, Matthew Beach, Yiheng Duan, Xiuzhe (Roger) Luo, Hsin-Yuan Huang, Giacomo Torlai, Shahnawaz Ahmed, Nathan Kitoran, Korbinian Kottmann, Di Luo, Hong-Ye Hu for valuable comments and inspiring discussions.

- 
- [1] Scott Aaronson. Shadow tomography of quantum states. *SIAM Journal on Computing*, 49(5):STOC18–368, 2019.
  - [2] Shahnawaz Ahmed, Carlos Sánchez Muñoz, Franco Nori, and Anton Frisk Kockum. Quantum state tomography with conditional generative adversarial networks. *Physical Review Letters*, 127(14):140502, 2021.
  - [3] Ahmed A Akhtar, Hong-Ye Hu, and Yi-Zhuang You. Scalable and flexible classical shadow tomography with tensor networks. *arXiv preprint arXiv:2209.02093*, 2022.
  - [4] Tameem Albash and Daniel A Lidar. Adiabatic quantum computation. *Reviews of Modern Physics*, 90(1):015002, 2018.
  - [5] Yuri Alexeev, Dave Bacon, Kenneth R Brown, Robert Calderbank, Lincoln D Carr, Frederic T Chong, Brian DeMarco, Dirk Englund, Edward Farhi, Bill Fefferman, et al. Quantum computer systems for scientific discovery. *PRX Quantum*, 2(1):017001, 2021.
  - [6] Ehud Altman, Kenneth R Brown, Giuseppe Carleo, Lincoln D Carr, Eugene Demler, Cheng Chin, Brian DeMarco, Sophia E Economou, Mark A Eriksson, Kai-Mei C Fu, et al. Quantum simulators: Architectures and opportunities. *PRX Quantum*, 2(1):017003, 2021.
  - [7] Sanjeev Arora, Simon S Du, Wei Hu, Zhiyuan Li, Russ R Salakhutdinov, and Ruosong Wang. On exact compu-

- tation with an infinitely wide neural net. *Advances in Neural Information Processing Systems*, 32, 2019.
- [8] Jimmy Lei Ba, Jamie Ryan Kiros, and Geoffrey E Hinton. Layer normalization. *arXiv preprint arXiv:1607.06450*, 2016.
  - [9] Ville Bergholm, Josh Izaac, Maria Schuld, Christian Gogolin, M Sohaib Alam, Shahnawaz Ahmed, Juan Miguel Arrazola, Carsten Blank, Alain Delgado, Soran Jahangiri, et al. PennyLane: Automatic differentiation of hybrid quantum-classical computations. *arXiv preprint arXiv:1811.04968*, 2018.
  - [10] Hannes Bernien, Sylvain Schwartz, Alexander Keesling, Harry Levine, Ahmed Omran, Hannes Pichler, Soonwon Choi, Alexander S Zibrov, Manuel Endres, Markus Greiner, et al. Probing many-body dynamics on a 51-atom quantum simulator. *Nature*, 551(7682):579–584, 2017.
  - [11] Christian Berton, Jonas Haferkamp, Marcel Hinsche, Marios Ioannou, Jens Eisert, and Hakop Pashayan. Shallow shadows: Expectation estimation using low-depth random clifford circuits. *arXiv preprint arXiv:2209.12924*, 2022.
  - [12] Jeff Bezanson, Alan Edelman, Stefan Karpinski, and Viral B Shah. Julia: A fresh approach to numerical computing. *SIAM review*, 59(1):65–98, 2017.
  - [13] Dolev Bluvstein, Harry Levine, Giulia Semeghini, Tout T Wang, Sepehr Ebadi, Marcin Kalinowski, Alexander Keesling, Nishad Maskara, Hannes Pichler, Markus Greiner, et al. A quantum processor based on coherent transport of entangled atom arrays. *Nature*, 604(7906):451–456, 2022.
  - [14] Max Born and Vladimir Fock. Beweis des adiabaten-satzes. *Zeitschrift für Physik*, 51(3):165–180, 1928.
  - [15] Tom Brown, Benjamin Mann, Nick Ryder, Melanie Subbiah, Jared D Kaplan, Prafulla Dhariwal, Arvind Neelakantan, Pranav Shyam, Girish Sastry, Amanda Askell, Sandhini Agarwal, Ariel Herbert-Voss, Gretchen Krueger, Tom Henighan, Rewon Child, Aditya Ramesh, Daniel Ziegler, Jeffrey Wu, Clemens Winter, Chris Hesse, Mark Chen, Eric Sigler, Mateusz Litwin, Scott Gray, Benjamin Chess, Jack Clark, Christopher Berner, Sam McCandlish, Alec Radford, Ilya Sutskever, and Dario Amodei. Language models are few-shot learners. In H. Larochelle, M. Ranzato, R. Hadsell, M.F. Balcan, and H. Lin, editors, *Advances in Neural Information Processing Systems*, volume 33, pages 1877–1901. Curran Associates, Inc., 2020.
  - [16] Kieron Burke. Perspective on density functional theory. *The Journal of chemical physics*, 136(15):150901, 2012.
  - [17] Juan Carrasquilla, Di Luo, Felipe Pérez, Ashley Milsted, Bryan K Clark, Maksims Volkovs, and Leandro Aolita. Probabilistic simulation of quantum circuits using a deep-learning architecture. *Physical Review A*, 104(3):032610, 2021.
  - [18] Juan Carrasquilla and Roger G Melko. Machine learning phases of matter. *Nature Physics*, 13(5):431–434, 2017.
  - [19] Juan Carrasquilla, Giacomo Torlai, Roger G Melko, and Leandro Aolita. Reconstructing quantum states with generative models. *Nature Machine Intelligence*, 1(3):155–161, 2019.
  - [20] David Ceperley and Berni Alder. Quantum monte carlo. *Science*, 231(4738):555–560, 1986.
  - [21] Peter Cha, Paul Ginsparg, Felix Wu, Juan Carrasquilla, Peter L McMahon, and Eun-Ah Kim. Attention-based quantum tomography. *Machine Learning: Science and Technology*, 3(1):01LT01, 2021.
  - [22] G Mauro D’Ariano, Matteo GA Paris, and Massimiliano F Sacchi. Quantum tomography. *Advances in Imaging and Electron Physics*, 128:206–309, 2003.
  - [23] Jacob Devlin, Ming-Wei Chang, Kenton Lee, and Kristina Toutanova. Bert: Pre-training of deep bidirectional transformers for language understanding. *arXiv preprint arXiv:1810.04805*, 2018.
  - [24] Sepehr Ebadi, Alexander Keesling, Madelyn Cain, Tout T Wang, Harry Levine, Dolev Bluvstein, Giulia Semeghini, Ahmed Omran, J-G Liu, Rhine Samajdar, et al. Quantum optimization of maximum independent set using rydberg atom arrays. *Science*, page eabo6587, 2022.
  - [25] Sepehr Ebadi, Tout T Wang, Harry Levine, Alexander Keesling, Giulia Semeghini, Ahmed Omran, Dolev Bluvstein, Rhine Samajdar, Hannes Pichler, Wen Wei Ho, et al. Quantum phases of matter on a 256-atom programmable quantum simulator. *Nature*, 595(7866):227–232, 2021.
  - [26] Matthew Fishman, Steven R. White, and E. Miles Stoudenmire. The ITensor Software Library for Tensor Network Calculations. *SciPost Phys. Codebases*, page 4, 2022.
  - [27] Xun Gao and Lu-Ming Duan. Efficient representation of quantum many-body states with deep neural networks. *Nature communications*, 8(1):1–6, 2017.
  - [28] David Gross, Yi-Kai Liu, Steven T Flammia, Stephen Becker, and Jens Eisert. Quantum state tomography via compressed sensing. *Physical review letters*, 105(15):150401, 2010.
  - [29] Albert Gu, Karan Goel, and Christopher Re. Efficiently modeling long sequences with structured state spaces. In *International Conference on Learning Representations*, 2022.
  - [30] Hartmut Häffner, Wolfgang Hänsel, CF Roos, Jan Benhelm, D Chek-al Kar, M Chwalla, T Körber, UD Rapol, M Riebe, PO Schmidt, et al. Scalable multiparticle entanglement of trapped ions. *Nature*, 438(7068):643–646, 2005.
  - [31] Hong-Ye Hu, Soonwon Choi, and Yi-Zhuang You. Classical shadow tomography with locally scrambled quantum dynamics. *arXiv preprint arXiv:2107.04817*, 2021.
  - [32] Hsin-Yuan Huang, Richard Kueng, and John Preskill. Predicting many properties of a quantum system from very few measurements. *Nature Physics*, 16(10):1050–1057, 2020.
  - [33] Hsin-Yuan Huang, Richard Kueng, and John Preskill. Efficient estimation of pauli observables by derandomization. *Physical review letters*, 127(3):030503, 2021.
  - [34] Hsin-Yuan Huang, Richard Kueng, Giacomo Torlai, Victor V. Albert, and John Preskill. Provably efficient machine learning for quantum many-body problems. *Science*, 377(6613):eabk3333, 2022.
  - [35] Arthur Jacot, Franck Gabriel, and Clément Hongler. Neural tangent kernel: Convergence and generalization in neural networks. *Advances in neural information processing systems*, 31, 2018.
  - [36] Diederik P Kingma and Jimmy Ba. Adam: A method for stochastic optimization. *ICLR*, 2015.
  - [37] Thomas N. Kipf and Max Welling. Semi-supervised classification with graph convolutional networks. In *International Conference on Learning Representations*, 2017.

- [38] Yuhong Li, Tianle Cai, Yi Zhang, Deming Chen, and Debadeepta Dey. What makes convolutional models great on long sequence modeling? *arXiv preprint arXiv:2210.09298*, 2022.
- [39] Ze Liu, Yutong Lin, Yue Cao, Han Hu, Yixuan Wei, Zheng Zhang, Stephen Lin, and Baining Guo. Swin transformer: Hierarchical vision transformer using shifted windows. In *Proceedings of the IEEE/CVF International Conference on Computer Vision*, pages 10012–10022, 2021.
- [40] Ilya Loshchilov and Frank Hutter. SGDR: Stochastic gradient descent with warm restarts. In *International Conference on Learning Representations*, 2017.
- [41] Chao-Yang Lu, Xiao-Qi Zhou, Otfried Gühne, Wei-Bo Gao, Jin Zhang, Zhen-Sheng Yuan, Alexander Goebel, Tao Yang, and Jian-Wei Pan. Experimental entanglement of six photons in graph states. *Nature physics*, 3(2):91–95, 2007.
- [42] Di Luo, Zhuo Chen, Juan Carrasquilla, and Bryan K Clark. Autoregressive neural network for simulating open quantum systems via a probabilistic formulation. *Physical review letters*, 128(9):090501, 2022.
- [43] Cole Miles, Rhine Samajdar, Sepehr Ebadi, Tout T Wang, Hannes Pichler, Subir Sachdev, Mikhail D Lukin, Markus Greiner, Kilian Q Weinberger, and Eun-Ah Kim. Machine learning discovery of new phases in programmable quantum simulator snapshots. *arXiv preprint arXiv:2112.10789*, 2021.
- [44] Hao Peng, Nikolaos Pappas, Dani Yogatama, Roy Schwartz, Noah Smith, and Lingpeng Kong. Random feature attention. In *International Conference on Learning Representations*, 2021.
- [45] QuEra Computing Inc. Bloade.jl, 2022.
- [46] Andrea Rocchetto, Edward Grant, Sergii Strelchuk, Giuseppe Carleo, and Simone Severini. Learning hard quantum distributions with variational autoencoders. *npj Quantum Information*, 4(1):1–7, 2018.
- [47] CF Roos, GPT Lancaster, M Riebe, H Häffner, W Hänsel, S Gulde, C Becher, J Eschner, F Schmidt-Kaler, and R Blatt. Bell states of atoms with ultralong lifetimes and their tomographic state analysis. *Physical review letters*, 92(22):220402, 2004.
- [48] Rhine Samajdar, Wen Wei Ho, Hannes Pichler, Mikhail D. Lukin, and Subir Sachdev. Complex density wave orders and quantum phase transitions in a model of square-lattice rydberg atom arrays. *Phys. Rev. Lett.*, 124:103601, Mar 2020.
- [49] Pascal Scholl, Michael Schuler, Hannah J Williams, Alexander A Eberharter, Daniel Barredo, Kai-Niklas Schymik, Vincent Lienhard, Louis-Paul Henry, Thomas C Lang, Thierry Lahaye, et al. Quantum simulation of 2d antiferromagnets with hundreds of rydberg atoms. *Nature*, 595(7866):233–238, 2021.
- [50] Giulia Semeghini, Harry Levine, Alexander Keesling, Sepehr Ebadi, Tout T Wang, Dolev Bluvstein, Ruben Verresen, Hannes Pichler, Marcin Kalinowski, Rhine Samajdar, et al. Probing topological spin liquids on a programmable quantum simulator. *Science*, 374(6572):1242–1247, 2021.
- [51] Vaishaal Shankar, Alex Fang, Wenshuo Guo, Sara Fridovich-Keil, Jonathan Ragan-Kelley, Ludwig Schmidt, and Benjamin Recht. Neural kernels without tangents. In *International Conference on Machine Learning*, pages 8614–8623. PMLR, 2020.
- [52] Nitish Srivastava, Geoffrey Hinton, Alex Krizhevsky, Ilya Sutskever, and Ruslan Salakhutdinov. Dropout: a simple way to prevent neural networks from overfitting. *The journal of machine learning research*, 15(1):1929–1958, 2014.
- [53] Giacomo Torlai, Guglielmo Mazzola, Juan Carrasquilla, Matthias Troyer, Roger Melko, and Giuseppe Carleo. Neural-network quantum state tomography. *Nature Physics*, 14(5):447–450, 2018.
- [54] Giacomo Torlai, Brian Timar, Evert P. L. van Nieuwenburg, Harry Levine, Ahmed Omran, Alexander Keesling, Hannes Bernien, Markus Greiner, Vladan Vuletić, Mikhail D. Lukin, Roger G. Melko, and Manuel Endres. Integrating neural networks with a quantum simulator for state reconstruction. *Physical Review Letters*, 123:230504, 2019.
- [55] Rodrigo A Vargas-Hernández, John Sous, Mona Berciu, and Roman V Krems. Extrapolating quantum observables with machine learning: Inferring multiple phase transitions from properties of a single phase. *Physical review letters*, 121(25):255702, 2018.
- [56] Ashish Vaswani, Noam Shazeer, Niki Parmar, Jakob Uszkoreit, Llion Jones, Aidan N Gomez, Łukasz Kaiser, and Illia Polosukhin. Attention is all you need. *Advances in neural information processing systems*, 30, 2017.
- [57] K Vogel and H Risken. Determination of quasiprobability distributions in terms of probability distributions for the rotated quadrature phase. *Physical Review A*, 40(5):2847, 1989.
- [58] Jiangran Wang, Zhuo Chen, Di Luo, Zhizhen Zhao, Vera Mikyoung Hur, and Bryan K Clark. Spacetime neural network for high dimensional quantum dynamics. *arXiv preprint arXiv:2108.02200*, 2021.
- [59] Steven R White. Density matrix formulation for quantum renormalization groups. *Physical review letters*, 69(19):2863, 1992.
- [60] Yuan-Hang Zhang and Massimiliano Di Ventra. Transformer quantum state: A multi-purpose model for quantum many-body problems. *arXiv preprint arXiv:2208.01758*, 2022.



## Appendix A: Model Structures

### 1. Transformer

Transformer networks constitute a powerful class of sequence models that use attention mechanisms as their central building blocks, and this structure has also been applied in various sub-fields of physics [17, 21, 42, 58]. In this work, we closely follow the original proposal of transformer networks [56], adopting the standard encoder-only transformer architecture. The network consists of an embedding layer, followed by a sequence of  $N$  decoder blocks with self-attention modules.

*a. Embedding and Positional Encoding.* The transformer architecture uses learned embeddings that linearly map one-hot encoded input tokens to vectors of dimension  $d_{\text{model}}$ . After the embedding, positional information is injected via a positional encoding layer. This mechanism allows the model to make use of the relative and absolute positions of tokens in a sequence. The positional encodings are given by sine and cosine functions of different frequencies and are functions of the dimension and position  $k$  in the sequence

$$pe(k, 2i) = \sin\left(\frac{k}{10000^{2i/d_{\text{model}}}}\right), \quad pe(k, 2i + 1) = \cos\left(\frac{k}{10000^{2i/d_{\text{model}}}}\right), \quad (\text{A1})$$

where  $i$  refers to the dimension. After embedding and positional encoding, the first component of a decoder block is the self-attention mechanism.

*b. Multi-head Self-Attention.* An attention function can be described as mapping a query  $Q$  and a set of key-value pairs  $K, V$  to an output which is computed as a weighted sum with weights based on the query and key. The specific attention function used in the transformer architecture is called scaled dot-product attention and is given by the function

$$\text{Attention}(Q, K, V) = \text{softmax}\left(\frac{QK^T}{\sqrt{d_k}}\right) V, \quad (\text{A2})$$

where  $Q, K$  and  $V$  are linear transformations of the input vectors

$$Q = XW_Q, \quad K = XW_K, \quad V = XW_V \quad (\text{A3})$$

where  $X \in \mathbb{R}^{n \times d_{\text{model}}}$  is the matrix of the  $n$  embedded input tokens with dimension  $d_{\text{model}}$ . As in Ref. [56], we use multi-head-attention where the input vectors are linearly projected  $n_h$  times to query, key, and value vectors resulting in  $n_h$  attention vectors. These are then concatenated and again projected so that the final output of the multi-head self-attention module is

$$\begin{aligned} \text{Multi-head}(Q, K, V) &= \text{Concat}(\text{head}_1, \dots, \text{head}_{n_h}) \\ \text{where head}_i &= \text{Attention}(Q_i, K_i, V_i) \end{aligned} \quad (\text{A4})$$

with  $Q_i = XW_Q^{(i)}$ ,  $K_i = XW_K^{(i)}$  and  $V_i = XW_V^{(i)}$ .

*c. Position-wise Feedforward.* After the multi-head attention layer, we have a position-wise feedforward network, which is a fully connected neural network with two linear transformations and a ReLU activation in between, applied to each position separately and identically.

Besides, each sublayer (i.e., self-attention or position-wise feedforward) has a residual connection and is followed by layer normalization, resulting in the transform  $\text{LayerNorm}(x + \text{SubLayer}(x))$ . Finally, after the last transformer block, the output is passed through a linear projection and a softmax layer.

### 2. Conditioning Network

In our proposed model structure, there is a conditioning network that takes the classical description of a quantum system and outputs a representation of this system. As we show in Fig. 2 and 7, one may choose different network architectures suitable for various types of quantum systems. Here we explain our two choices of conditioning network structures, graph neural networks (GNN) and linear models, for the problems of 2D random Heisenberg models and Rydberg atom systems, respectively.

*a. Graph Neural Network (GNN)*

In this paper, we adopt one of the most popular GNN structures, Graph Convolution Network (GCN) [37], as the conditioning network for 2D random Heisenberg models. Given a weighted undirected graph  $\mathcal{G}$  with  $n$  nodes and the adjacency matrix  $A$ , the GCN consists of  $L$  graph convolutional layers. The  $(l+1)$ -th layer is given by

$$H^{(l+1)} = \text{ReLU} \left( \tilde{D}^{-\frac{1}{2}} \tilde{A} \tilde{D}^{-\frac{1}{2}} H^{(l)} W^{(l)} \right) \quad (\text{A5})$$

where  $\tilde{A} = A + I_N$  ( $I_N$  is the identity matrix),  $\tilde{D}$  is a diagonal matrix with  $\tilde{D}_{ii} = \sum_j \tilde{A}_{ij}$ ,  $W^{(l)}$  is a layer-specific trainable weight matrix,  $\text{ReLU}(\cdot) = \max(0, \cdot)$  is an activation function and  $H^{(l)} \in \mathbb{R}^{N \times D}$  is the output of the  $l$ -th layer. In our implementation,  $H^{(0)} = X$ , where  $X \in \mathbb{R}^{N \times 1}$  with the  $i$ -th element as the weighted degree of the  $i$ -th node. After passing the graph  $\mathcal{G}$  through the graph convolutional layers, we obtain node embeddings  $z_1, \dots, z_n$ , i.e., the rows of  $H^L$ . Subsequently, we apply a linear projection, with trainable weights  $\{W_i\}_{i \in [n]}$ , on the embeddings to obtain an encoding that will be fed to the transformer,

$$z_1, \dots, z_n \mapsto \sum_{i=1}^n W_i z_i. \quad (\text{A6})$$

*b. Linear Model*

For Rydberg atom systems, since the classical description of a system is just a set of scalars, we find that a linear model suffices for the conditioning network. For instance, for a Rydberg atom system with  $K$  system parameters, we concatenate the parameters into a vector  $\mathbf{x} \in \mathbb{R}^K$ , and apply the linear transformation

$$\mathbf{x} \mapsto W\mathbf{x} + b \quad (\text{A7})$$

where  $W$  is a trainable weight matrix and  $b$  is a trainable bias term.

## Appendix B: Experimental details

### 1. 2D anti-ferromagnetic random Heisenberg model

For 2D random Heisenberg models, our transformer-based generative model is trained for 100 epochs with mini-batches of size 100, using the Adam Optimizer [36]. We varied the learning rate using 5 warmup epochs, increasing the learning rate from 0 to  $1\text{e-}3$ , followed by a cosine decay with a maximum learning rate set to  $1\text{e-}3$  and final learning rate set to  $1\text{e-}7$ . We use dropout regularization with a dropout rate 0.1 [52]. In the transformer architecture, we use 4 decoder blocks, with 4 attention heads and model dimensionality set to 128. The graph neural network consists of 3 graph convolutional layers with ReLU activations and with hidden sizes 64, 32, and 16, respectively. After the GCN layers, a linear transformation is applied to each position separately, with dimension 128 (equal to the transformer dimension). All models are trained for approximately 2.5 hours on a single NVIDIA TITAN Xp GPU with 12GB of memory.

### 2. Rydberg atom systems

*a. Hyper-parameters*

For Rydberg atom systems, our transformer-based generative model is trained for 20k-50k iterations with mini-batches of size 512, using the Adam Optimizer. We initialize the learning rate with  $1\text{e-}3$ , followed by a cosine decay with the final learning rate set to  $1\text{e-}7$ . We use dropout regularization with a dropout rate 0.1. In the transformer, we use 4 decoder blocks with 4 attention heads and model dimensionality set to 128. Each model is trained on a single GPU, which is either an NVIDIA V100 or NVIDIA A6000. 10k iterations take about 1 hour on a single GPU.

*b. Order Parameters*

**1D Lattices.** Inspired by Ref. [10], we define the order parameters for the  $Z_2$  and  $Z_3$  ordered phases as  $O_{Z_2}$  and  $O_{Z_3}$

$$O_{Z_2} = \frac{1}{n} \sum_{i=1,3,5,\dots} N_i \quad (\text{B1})$$

$$O_{Z_3} = \frac{1}{n} \sum_{i=1,4,7,\dots} N_i \quad (\text{B2})$$

where  $n$  is the number of atoms.

The design of these order parameters is quite intuitive. For example, consider the 7-atom 1D lattice shown in Fig. 6: in the  $Z_2$  ordered phase, the expectation value of  $O_{Z_2}$  should be very high (upper bounded by 1), since atoms at sites 1, 3, 5, ... are excited with high probability; in the  $Z_3$  ordered phase, the expectation value of  $O_{Z_3}$  should be very high (upper bounded by 1), since atoms at sites 1, 4, 7, ... are excited with high probability.

Similar to the practice in Ref. [34], we set thresholds on the values of these order parameters to determine the phase of a state: If  $\langle O_{Z_2} \rangle > 0.7$ , we determine this state as in the  $Z_2$  ordered phase; if  $\langle O_{Z_2} \rangle > 0.6$ , we determine the state as in the  $Z_3$  ordered phase; if a state is not in one of these phases, we classify it as in the disordered phase.

**2D Square Lattices.** Following Ref. [25], we define the order parameters for 2D square lattices of Rydberg atoms using the Fourier transformation. Specifically, we apply the Fourier transformation to single-shot measurement outcomes as

$$\mathcal{F}(\mathbf{k}) = \left| \sum_i \exp(i\mathbf{k} \cdot \vec{x}_i/a) N_i / \sqrt{n} \right| \quad (\text{B3})$$

where  $n$  is the number of atoms. Then, we use the symmetric Fourier transform

$$\tilde{\mathcal{F}}(k_1, k_2) = \mathcal{F}(k_1, k_2) + \mathcal{F}(k_2, k_1)/2 \quad (\text{B4})$$

to take the reflection symmetry into consideration.

Following Ref. [25] defines the order parameters for the Checkboard and Striated phases as

$$O_{\text{checkboard}} = (\mathcal{F}(\pi, \pi) - \tilde{\mathcal{F}}(\pi, 0))/1.6 \quad (\text{B5})$$

$$O_{\text{striated}} = (\tilde{\mathcal{F}}(\pi, 0) - \tilde{\mathcal{F}}(\pi/2, \pi))/0.8 \quad (\text{B6})$$

where we involve the normalization factors 1.6 and 0.8 (that Ref. [25] did not use) to normalize the two order parameters so that their values are upper bounded by 1.

For the Staggered phase, [25] has not defined its corresponding order parameter, so we define it by ourselves based on our observation of its patterns in the Fourier space:

$$O_{\text{staggered}} = (\mathcal{F}(\pi/2, \pi/2) + \mathcal{F}(-\pi/2, \pi/2) + \mathcal{F}(\pi/2, -\pi/2) + \mathcal{F}(-\pi/2, -\pi/2)) / 4 \quad (\text{B7})$$

which is also upper-bounded by 1.

For each prepared state, we apply  $\{O_{\text{checkboard}}, O_{\text{striated}}, O_{\text{staggered}}\}$  to it over measurement outcomes to estimate the values of these order parameters,  $\{\langle O_{\text{checkboard}} \rangle, \langle O_{\text{striated}} \rangle, \langle O_{\text{staggered}} \rangle\}$ . Then, we use a threshold 0.65 to determine the phase: if one of  $\{\langle O_{\text{checkboard}} \rangle, \langle O_{\text{striated}} \rangle, \langle O_{\text{staggered}} \rangle\}$  is above this threshold, we determine the state as in the corresponding phase; if all values are below the threshold, we determine the state as in the disordered phase; otherwise, if multiple order parameters are above the threshold (very rare situation), we use the one with the largest value to determine the phase.

In Fig. 13, we provide a visualization of the Fourier spectra of the three ordered phases. One can see each Fourier spectrum has some dominant peaks, which can be viewed as the signatures of each phase. In fact, the design of order parameters in Ref. [25] is based on this intuition. Notably, since our numerical study is conducted on 5x5 square lattices, the Staggered phase is a little different from the observation in Ref. [48] due to finite-system-size effects, so our Fourier space visualization of the Staggered phase is also different from that of Ref. [48]. Hence, when studying 2D square lattices beyond the size of 5x5, one should modify our choice of  $O_{\text{staggered}}$  in Eq. (B7) correspondingly.

## Appendix C: Classical Simulation

### 1. 2D Random Heisenberg Models

For 2D random Heisenberg systems with fewer than 20 qubits, we generate 100 random Hamiltonians by sampling coupling constants  $J_{ij} \sim \mathcal{U}[0, 2]$ , and determine their ground states via exact diagonalization. After obtaining the

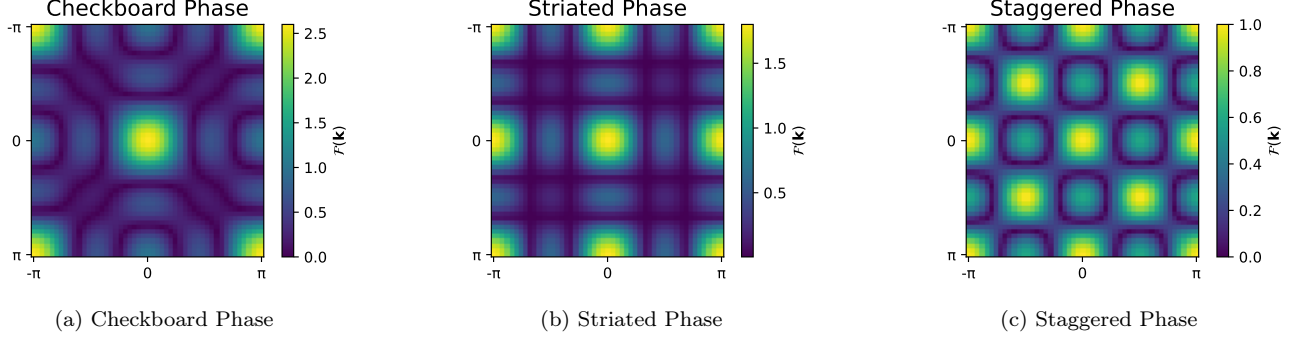


FIG. 13. The Fourier space visualization of 2D Rydberg square lattices in different ordered phases (see Fig. 6 for illustration of these phases).

ground state wavefunction, we apply Pauli-6 POVM measurements to it repeatedly following the classical shadow protocol [32], which effectively corresponds to measuring the state in random Pauli bases. For 2D random Heisenberg systems with 20 qubits or more, we use the publicly available dataset provided by the authors of Ref. [34] (<https://github.com/hsinyuan-huang/provable-ml-quantum>), where the ground states are approximated by DMRG using the ITensor package[26]. Our implementation is written in Python and partially built on the PennyLane library [9].

#### Pauli-6 POVM

The single-qubit Pauli-6 POVM has six outcomes corresponding to sub-normalized rank-1 projections

$$\mathcal{M}_{\text{Pauli-6}} = \left\{ \frac{1}{3}|+\rangle\langle+|, \frac{1}{3}|-\rangle\langle-|, \frac{1}{3}|+i\rangle\langle+i|, \frac{1}{3}|-i\rangle\langle-i|, \frac{1}{3}|0\rangle\langle 0|, \frac{1}{3}|1\rangle\langle 1| \right\} \quad (\text{C1})$$

where  $\{|+\rangle, |-\rangle\}$ ,  $\{|+i\rangle, |-i\rangle\}$  and  $\{|0\rangle, |1\rangle\}$  are the eigenbases of the Pauli operators  $X$ ,  $Y$  and  $Z$ , respectively. Since each Pauli matrix and, in addition, the identity matrix, can be obtained from real linear combinations of the projections in  $\mathcal{M}_{\text{Pauli-6}}$ , it follows that the single-qubit Pauli-6 POVM spans the space of  $2 \times 2$  Hermitian matrices. The Pauli-6 POVM on  $n$  qubits is formed by taking  $n$ -fold tensor products of the POVM elements in  $\mathcal{M}_{\text{Pauli-6}}$  and is hence informationally complete.

## 2. Rydberg Atom Systems

Our classical simulations of Rydberg atom systems are conducted via the Bloqade.jl [45], a Julia [12] package, with the following steps:

1. We construct a 1D or 2D lattice of Rydberg atoms with a specified lattice configuration (e.g., lattice dimensions and atom separation  $a$ ).
2. We design schedulers for the adiabatic evolution of  $\Omega$  and  $\Delta$  (defined in Eq. (8)), respectively. We visualize the schedulers we used in Fig. 14.
3. We start the simulation of adiabatic evolution via an ODE solver. At some preset time steps, we pause the simulation, and apply  $Z$ -basis measurements to this lattice. Then, we record the measurement outcomes along with the current values of  $\Omega$  and  $\Delta$ , and resume the simulation process.

**Remarks.** Bloqade.jl[45] considers neutral  $^{87}\text{Rb}$  atoms as the Rydberg atoms, with the  $70S_{1/2}$  Rydberg state of Rb atoms as the excited state  $|r\rangle$ . Then, the Rydberg interaction constant becomes  $V_0 = 862690 \times 2\pi \text{ MHz } \mu\text{m}^6$  ( $V_0$  is also often referred to as  $C_6$  in the literature).



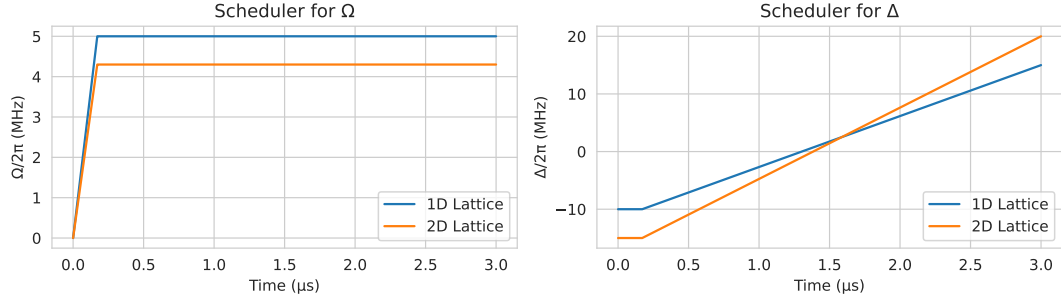


FIG. 14. Our schedulers for  $\Omega$  and  $\Delta$  during an adiabatic evolution of  $3\mu$ s, for 1D and 2D lattices of Rydberg atoms. For longer or shorter adiabatic evolution times, we just proportionally enlarge or shrink these schedules.